

Highly optimized empirical potential model of silicon

Thomas J Lenosky[†], Babak Sadigh[†], Eduardo Alonso[†], Vasily V Bulatov[†],
Tomas Diaz de la Rubia[†], Jeongnim Kim[‡], Arthur F Voter[§] and Joel D Kress[§]

[†] Lawrence Livermore National Laboratory, Livermore, CA 94551, USA

[‡] Department of Physics, Ohio State University, Columbus, OH 43210, USA

[§] Theoretical Division, Los Alamos National Laboratory, Los Alamos, NM 87545, USA

Received 4 May 2000, accepted for publication 5 September 2000

Abstract. We fit an empirical potential for silicon using the modified embedded atom (MEAM) functional form, which contains a nonlinear function of a sum of pairwise and three-body terms. The three-body term is similar to the Stillinger–Weber form. We parametrized our model using five cubic splines, each with 10 fitting parameters, and fitted the parameters to a large database using the force-matching method. Our model provides a reasonable description of energetics for all atomic coordinations, Z , from the dimer ($Z = 1$) to fcc and hcp ($Z = 12$). It accurately reproduces phonons and elastic constants, as well as point defect energetics. It also provides a good description of reconstruction energetics for both the 30° and 90° partial dislocations. Unlike previous models, our model accurately predicts formation energies and geometries of interstitial complexes—small clusters, interstitial-chain and planar $\{311\}$ defects.

1. Introduction

Short-ranged classical interatomic potentials are of great importance for atomistic modelling of large-scale phenomena in materials science. They naturally scale linearly with the number of atoms in a calculation and thus allow for million-atom simulations of e.g. grain boundaries and dislocations. In general it is difficult to derive a potential from first principles, although some progress has been made [1]; instead, another methodology is to try to devise a reasonable functional of the environment of an atom with a number of parameters which are fitted to experimental results or to accurate quantum mechanical calculations.

The earliest classical potentials, mainly used for the study of liquids, only contained contributions from pair interactions. However, early on it was realized that pair potentials lack certain fundamental properties required for the accurate description of chemical and metallic bonding. One of the early successful attempts to include many-body effects in the description of the latter was the introduction of the embedding functional [2], which depends nonlinearly upon the coordination number of each atom. This development led to the birth of the embedded-atom method (EAM) [3], which utilizes a pairwise embedding functional, comparable in computational efficiency to simple pair potential models. EAM has thus provided a simple framework for the accurate description of noble transition metals and their alloys, involving relatively few fitting parameters. However, going beyond pairwise embedding functionals seems to be necessary to describe early transition metal systems, which generally are body-centred cubic in their ground state.

At about the same time, major progress was made in the field of semiconductor physics through the work of Stillinger and Weber [4]. They constructed a model (SW) that describes

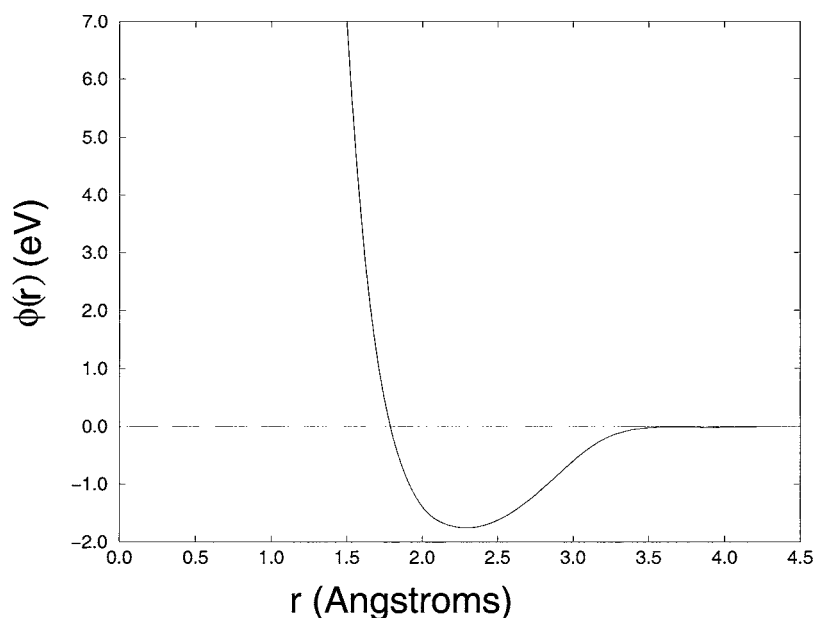


Figure 1. The pair potential $\phi(r)$.

the covalent bonding in silicon by going beyond pair potentials and including a three-body angular term. This potential, although 15 years old, is still the most commonly used model for silicon.

Given the successful development of the EAM and SW, it was hoped that a mixture of the two ideas would result in a generic formalism capable of producing transferable potentials for any system. Thus incorporating angular terms in the EAM pair functional led to the development of the modified embedded-atom method (MEAM). MEAM models have already been constructed for several elements [5, 6]. An alternative approach has been proposed by Pasianot *et al* [7] in which the angular term is outside the pair functional. While these combined forms have not yet found the wide audience of EAM and SW, the general approach looks promising. In the MEAM potentials constructed so far, the fitting procedure was intentionally restricted to a small number of parameters. While this approach maintains an appealing simplicity, it necessarily limits the accuracy.

Our goal in this paper is to explore the limits of accuracy available with a more general fitting approach using the MEAM form. We fit a model with many degrees of freedom to a large database of first principles and experimental data. Our goal is eventually to devise a framework for constructing accurate empirical potentials for any system. As a first case, we have chosen to develop a model for silicon. It is an element of enormous technological importance. Grain boundaries, surface reconstructions and dislocation lines present examples where understanding of atomistic processes becomes important as silicon devices are fabricated at ever-decreasing length scales. Density functional theory provides a highly accurate framework for atomistic calculations, but is currently unable to treat more than a few hundred atoms.

Many empirical potentials have been fitted for silicon (see review in [8] and [4, 9–12]). Most recently, the environment-dependent interatomic potential (EDIP) [11, 12] was proposed as an improvement over the previous models. Whenever possible, we compare the quality of

our optimized model with these previous works. In the next section, we will describe in detail the form and the fitting procedure of the potential, and in section 3 we investigate the accuracy of this model as compared to other empirical potentials.

2. Construction of the model

In this work, we have fitted a new interatomic potential for silicon that offers generally improved accuracy over previously proposed models, while being no more expensive to evaluate. We have followed an identical fitting methodology to that used in a previous work [13] in which a high-quality orthogonal tight-binding model was fitted for silicon, but omitted some fitting data (Grüneisen parameter values and (100) surface energetics). We performed least-squares fits to the remaining database, which consisted of *ab initio* force and energy data on two- to five-atom clusters, liquid and amorphous systems, as well as experimental elastic constants and phonon frequencies. We also included calculated *ab initio* LDA (local density approximation) energetics for vacancy and interstitial point defects in the fit. One additional change in the data set was made: we modified the point defect energetics to reflect newer LDA values, which we describe later. The relative weights of the various data elements in the fit were the same as in our previous study. The concept of fitting to a database which includes forces is the ‘force matching’ method originally proposed by Ercolessi and Adams [14]. It has been successfully applied to fitting potentials for Al [14], Mg [15], Al–Mg [16], Al–Cu [17] and Al–Pb [18].

We have chosen the following functional form for our potential:

$$E = \sum_{ij} \phi(r_{ij}) + \sum_i U \left[\sum_j \rho(r_{ij}) + \sum_{jk} f(r_{ij}) f(r_{ik}) g(\cos(\theta_{jik})) \right] \quad (2.1)$$

where θ_{jik} is the angle centred on atom i . The pair potential $\phi(r)$ is summed over every independent pair of atoms, i.e. each pair is only counted once. Likewise, for the sum over j and k , each independent pair of atoms j and k is counted once. This form is identical to the MEAM form proposed by Baskes [6] for silicon, and contains as a special case the SW form ($U(x) \propto x$ and $\rho = 0$), and the EAM form ($f = 0$ or $g = 0$). Our MEAM model is different from the Baskes MEAM model in two respects: first, in the Baskes model d^2U/dx^2 is positive, while it is generally negative for our model; second, the Baskes model severely restricts the form of the functions in the potential. This final restriction is most evident in that $g(\cos(\theta))$ is expanded in powers of $\cos(\theta)$ in the Baskes model, so that $g(\cos(\theta)) = A_1 \cos(\theta) + A_2 \cos^2(\theta) + A_3 \cos^3(\theta)$. In our form, we represented g , ϕ , ρ , U , and f as cubic splines, each with 10 degrees of freedom. ϕ has a second-neighbour cutoff (4.5 Å), while ρ and f have first-neighbour cutoffs (3.5 Å). The domain of the functions U and g was set by the maximum extent of the fitting data. When evaluation of the potential leads to arguments of these functions past their endpoints, as is sometimes the case, we prescribe linear extrapolation to the needed point. The procedure for evaluating the splines is given in [19]. We give the parameters for the potential in table 1 and the functions are plotted in figures 1–5. These functions are relatively smooth (although their derivatives are less so), a necessary feature for a physically meaningful potential.

We fitted equation (2.1) with the least-squares technique using both the simplex simulated annealing scheme [19] as well as the Powell least-squares method [20]. Each fit took only a few minutes of workstation time, but many fits were necessary in order to obtain a good potential; we found the quality of our results to be highly dependent on the radial cutoffs of the model. Our best fit was obtained with the pair-potential $\phi(r)$ in equation (2.1), extending to 4.5 Å. Changing the radial cutoff for this quantity from 4.5 to 4.45 Å yielded a significantly worse fit. We also experimented a great deal with the number of intervals used for our cubic

Table 1. Parameters that specify the five cubic splines that comprise the potential. The first part of the table gives values at equally spaced spline knots defined by $t = (1 - \alpha)t_{\min} + \alpha * t_{\max}$ where $\alpha = i/N$ and N is the maximum value of the integer i . The middle part of the table gives derivatives of the splines at their endpoints. Finally, values of t_{\min} , t_{\max} , and N are given in the lowest part of the table.

i	$\phi(r_i)$ (eV)	$\rho(r_i)$	$f(r_i)$	$U((\rho_{\text{tot}})_i)$ (eV)	$g((\cos(\theta))_i)$
0	6.929 94	0.137 47	1.250 31	-1.074 93	5.254 16
1	-0.439 95	-0.148 31	0.868 21	-0.200 45	2.359 15
2	-1.701 23	-0.559 72	0.608 46	0.414 22	1.195 95
3	-1.624 73	-0.731 10	0.487 56	0.879 39	1.229 95
4	-0.996 96	-0.762 83	0.441 63	1.266 89	2.035 65
5	-0.273 91	-0.729 18	0.376 10	1.629 98	3.424 74
6	-0.024 99	-0.666 20	0.271 45	1.977 38	4.948 59
7	-0.017 84	-0.573 28	0.148 14	2.396 18	5.617 99
8	-0.009 61	-0.406 90	0.048 55		
9	0.0	-0.166 62	0.0		
10		0.0			
i	$(\phi(r))'$ (\AA^{-1} eV)	$(\rho(r))'$ (\AA^{-1})	$(f(r))'$ (\AA^{-1})	$(U(\rho_{\text{tot}}))'$ (eV)	$(g(\cos(\theta)))'$
0	-42.66967	-1.0	-3.618 94	0.735 14	-13.950 42
N	0.0	0.0	0.0	0.616 52	1.134 62
Spline	t	t_{\min}	t_{\max}	N	
ϕ	r (\AA)	1.5	4.5	9	
ρ	r (\AA)	1.5	3.5	10	
f	r (\AA)	1.5	3.5	9	
U	ρ_{tot}	-1.770 93	7.908 52	7	
g	$\cos(\theta)$	-1.0	0.800 14	7	

splines. A large number of intervals can give a good fit, but it introduces spurious oscillations in the potential, making it unphysical.

There are various transformations which leave our potential unchanged. In particular, the substitutions $\rho_1(r) = \alpha\rho(r)$, $U_1(x) = U(x/\alpha)$, $g_1(\cos(\theta)) = \alpha\beta^2g(\cos(\theta))$, and $f_1(r) = f(r)/\beta$ have no effect for any nonzero α and β , when ρ , U , g and f are replaced by ρ_1 , U_1 , g_1 and f_1 . These rescaling operations effectively reduce the number of parameters in our model from 50 to 49. We chose the sign of α to make the relationship with SW manifest: $U(x)$ is basically proportional to x , so as for SW, the three-body term in our model serves to penalize deviations from the tetrahedral angle. A three-body expansion about the tetrahedral angle is an excellent approximation for a tetrahedrally bonded covalent solid like Si. In fact, to within a few per cent, $U(x) \sim 0.49x - 0.054x^2 + 0.0039x^3$. The quadratic and cubic terms in this expansion can be viewed as a slight perturbation to the SW form.

For the cubic diamond structure the various energy terms in our potential are comparable in magnitude. The cohesive energy $E_{\text{coh}} = 2\phi(r_1) + 6\phi(r_2) + U(x_{\text{eq}})$, where r_1 is the nearest-neighbour distance, r_2 is the second nearest-neighbour distance, and x_{eq} is the argument of U for the equilibrium structure. We find $2\phi(r_1) = -3.48$ eV, $6\phi(r_2) = -0.11$ eV, and $U(x_{\text{eq}}) = -1.02$ eV. Furthermore, $x_{\text{eq}} = 4\rho(r_1) + 6f(r_1)^2g(-1/3)$, and we find that $4\rho(r_1) = -3.04$ while $6f(r_1)^2g(-1/3) = 1.34$, so these terms are also comparable in magnitude. Finally, x_{eq} is -1.70 , and is negative. Thus, unlike for EAM, x cannot be interpreted as an electronic density.

That the argument of U is not a physical density is also illustrated by the fact that $\rho(r)$ is not a monotonic function of r , but rather has a minimum near the nearest-neighbour distance

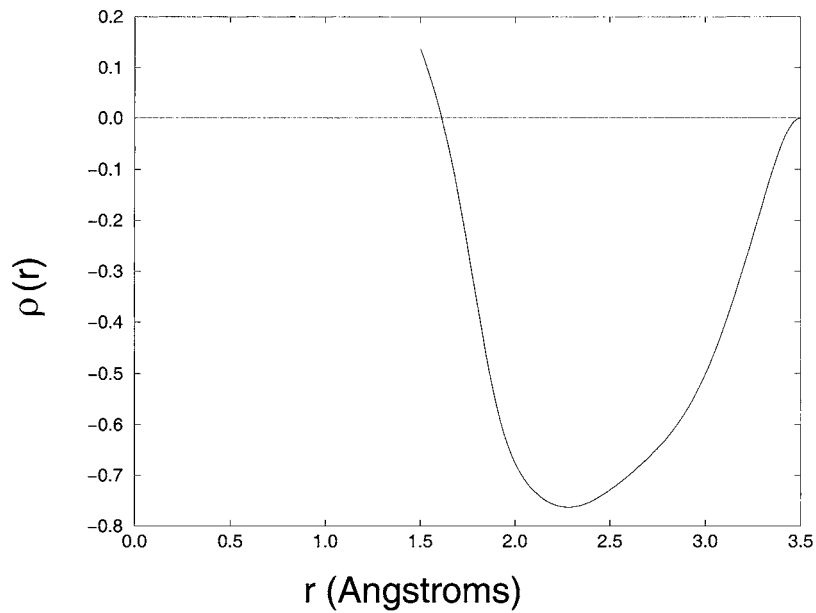


Figure 2. The embedding contribution $\rho(r)$.

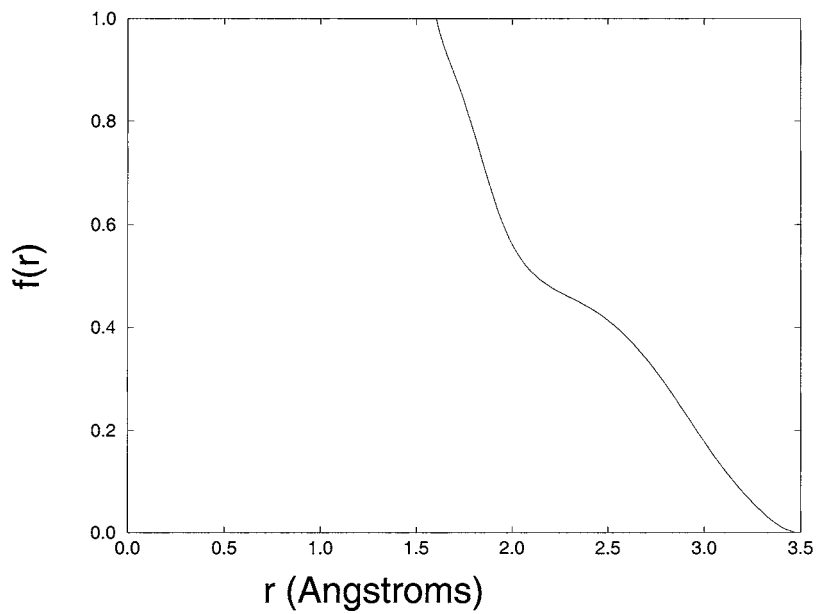


Figure 3. The radial cutoff function $f(r)$.

$r_1 = 2.351 \text{ \AA}$. Near r_1 , $\phi(r)$ also has a minimum that helps stabilize crystalline Si at its correct bond length. The function $f(r)$ decreases monotonically in r , as does the corresponding function in the SW model. It has an unusual change in slope for $r < 2 \text{ \AA}$, at distances which are found only in highly compressed structures. While $g(\cos(\theta))$ approximates an expansion around the tetrahedral angle ($\cos(\theta) = -1/3$), it has additional structure not seen in the SW model: it is neither quadratic nor does it equal zero at its minimum.

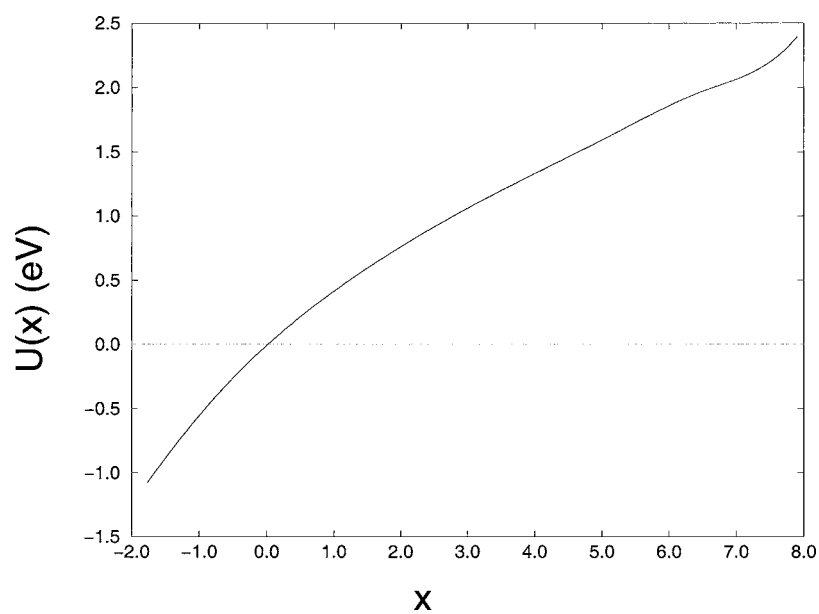


Figure 4. The embedding potential $U(\rho_{\text{tot}})$.

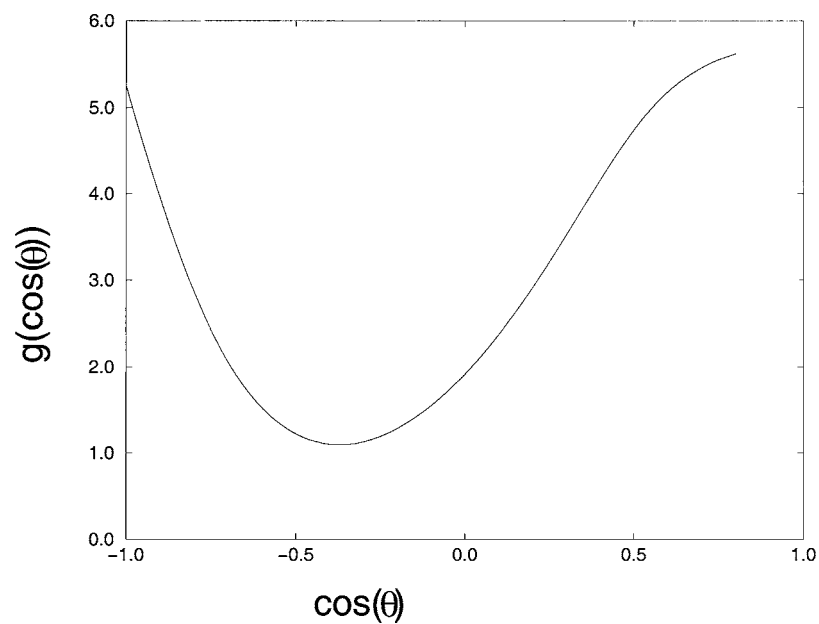


Figure 5. The three-body angular term $g(\cos(\theta))$.

3. Calculated properties

In this section we compare our model with several other approaches: EDIP, the recent state-of-the-art interatomic silicon potential [11, 12]; the Tersoff model, a previous state-of-the-art model [9]; a previous tight-binding model [13]; and where possible *ab initio* calculations and

Table 2. Silicon properties obtained from experiment, and calculated with our model, EDIP, the Tersoff model, the SW model and the tight-binding model (L = longitudinal, T = transverse, O = optical, A = acoustic).

	Experiment	Our model	EDIP ^a	Tersoff	SW	Tight-binding ^b
Lattice constant a (Å)	5.429 ^c	5.431	5.43	5.43 ^d	5.43 ^a	5.4287
Binding energy e (eV/atom)	4.63 ^e	4.612	4.65	4.63 ^d	4.63 ^a	4.620
Elastic constants						
B (Mbar)	0.978 ^f	1.100	0.99	0.98 ^d	0.98 ^a	1.001
$C_{11}-C_{12}$ (Mbar)	1.012 ^f	0.831	1.13	0.67 ^d	0.79 ^a	1.008
C_{44} (Mbar)	0.796 ^f	0.717	0.71	0.69 ^d	0.60 ^a	0.754
Phonon frequencies						
LTO(Γ) (THz)	15.53 ^f	15.08		16.1 ^g	17.8 ^g	15.58
TA(X) (THz)	4.49 ^f	7.16		6.91 ^g	6.65 ^g	5.16
TO(X) (THz)	13.90 ^f	13.65		14.9 ^g	15.6 ^g	13.66
LOA(X) (THz)	12.32 ^f	12.40		12.2 ^g	13.0 ^g	11.85
Grüneisen parameters						
LTO(Γ)	0.98 ^h	1.15		1.32 ^g	0.80 ^g	1.14
TA(X)	-1.40 ^h	0.09		-0.20 ^g	-0.04 ^g	-1.41
TO(X)	1.50 ^h	1.58		1.60 ^g	0.89 ^g	1.43
LOA(X)	0.90 ^h	1.26		1.27 ^g	0.83 ^g	0.90

^a [12].^b [13].^c [41].^d [8].^e [42].^f [43].^g [21].^h [44].

experiments. Two versions of EDIP have been published [11, 12]; our comparisons are with the final version [12]. Three versions of the Tersoff model have been published, and all of our comparisons refer to the final version, sometimes denoted ‘Tersoff 3’ in the literature. The properties of the SW [4] and Tersoff [9] models have also been extensively tabulated in [8], and also compared to EDIP in [12]. Our comparisons will largely omit the SW model in the interest of brevity.

The diamond structure cohesive energy, lattice constant, elastic moduli, some phonon frequencies and Grüneisen parameter values are compared in table 2. To our knowledge phonon frequencies and Grüneisen parameter values have not been published for EDIP. These comparisons show that the lattice constant, cohesive energy, and elastic moduli for both our model and EDIP are reasonable. Our model also demonstrates an accurate fit for some phonon frequencies. The soft transverse acoustic phonon at X is described relatively poorly by our model, as is its corresponding Grüneisen parameter. We attribute this error to the limited range of the potential. The tight-binding model [13] predicts these properties more accurately, including the Grüneisen parameter values.

We have computed the coefficient of thermal expansion and the heat capacity as a function of temperature for our model, using the quasiharmonic approximation in which independent phonon modes are populated using a Bose–Einstein distribution; interactions between the modes are neglected. Both quantities are nearly identical to those predicted by the Tersoff model, as calculated in [21]; at high temperatures our model predicts the experimental heat

Table 3. Prediction of *ab initio* forces present in the fit. Our model was fitted, in part, to *ab initio* force data on amorphous, liquid and bulk silicon (containing one vacancy or one interstitial) at elevated temperature. Here we compare the root-mean-square (rms) forces present in the original data, F_{rms} , with the corresponding rms error our model makes in predicting those forces, R_{rms} .

	F_{rms} (eV \AA^{-1})	R_{rms} (eV \AA^{-1})	$R_{\text{rms}}/F_{\text{rms}}$ (%)
Amorphous	1.34	0.78	58
Liquid	1.45	0.78	54
Vacancy	1.32	0.34	26
Interstitial	1.39	0.33	24

Table 4. Prediction of crystal phase energetics. For each crystal phase the atomic coordination, Z , is given, together with the LDA value of the cohesive energy, and values computed using our model, EDIP and the Tersoff model. All energies are relative to the relaxed diamond structure, and each structure is fully relaxed.

Structure	Z	E (LDA) (eV atom $^{-1}$)	E (our model) (eV atom $^{-1}$)	E (EDIP) (eV atom $^{-1}$) ^a	E (Tersoff) (eV atom $^{-1}$) ^b
Diamond	4	0.0	0.0	0.0	0.0
Hexagonal diamond	4	0.016	−0.009	0.0	0.0
bc8	4	0.13 ^c	0.08		0.25
(34) clathrate	4	0.08 ^d	0.04		
(46) clathrate	4	— ^d	0.08		
bct5	5	0.23 ^e	0.18	0.26	
sc	6	0.35 ^a	0.29	0.53	0.32
β -tin	6	0.21 ^a	0.31	0.67	0.33
bcc	8	0.52 ^a	0.72	1.60	0.43
Simple hexagonal	8	0.24 ^c	0.23		0.47
fcc	12	0.57 ^a	0.70	1.84	0.76
hcp	12	0.55 ^a	0.67	0.93	0.76

^a [12].

^b [8].

^c [45].

^d [46].

^e [24].

capacity accurately, but it overestimates the thermal expansion coefficient by about 35% at $T = 1200$ K.

Another measure of our model is the quality of fit to the force data. The root-mean-square error in the force predictions for the model, applied to the fitting data, is tabulated in table 3. The vacancy and interstitial data are for a single vacancy and a single interstitial added to a 64-atom cell. These data were taken from Harris functional molecular dynamics runs and recomputed using LDA, as described in [13]. Notably, the force matching error is only 24–26% for the vacancy and interstitial cells. Since the phonon frequencies are the square root of the restoring forces, this result suggests that typical phonon frequencies have about 12% error. Although our errors of 54 and 58% on the liquid and amorphous data do appear to indicate a poor fit, the SW [4] and Tersoff [9] interatomic potentials give force-matching errors of over 100% on similar data [22]. The tight-binding model is a more accurate potential, as the force-matching [14, 22] errors are somewhat less (16–26% versus 24–58%).

We have compared the energetics of various crystal phases using our model, EDIP, Tersoff and LDA in table 4. Our model predicts the relative energy of various crystal phases much more accurately than EDIP, for coordinations varying from diamond ($Z = 4$) to fcc ($Z = 12$),

Table 5. Prediction of crystal phase volumes. For each crystal phase the atomic coordination, Z , is given, together with the equilibrium volume of the fully relaxed structure. Values are computed using our model, EDIP, SW and LDA. The experimental equilibrium volume for the diamond structure is $20.0 \text{ \AA}^3/\text{atom}$.

Structure	Z	V (LDA) ^a ($\text{\AA}^3/\text{atom}$)	V (our model) ($\text{\AA}^3/\text{atom}$)	V (EDIP) ^b ($\text{\AA}^3/\text{atom}$)	V (Tersoff) ^b ($\text{\AA}^3/\text{atom}$)	V (SW) ^b ($\text{\AA}^3/\text{atom}$)
Diamond	4	19.6	20.0	20.0	20.0	20.0
Hexagonal diamond	4		20.0	20.0	20.0	20.0
bc8	4	17.5	17.0			
(34) clathrate	4		22.9			
(46) clathrate	4		22.7			
bct5	5	16.3	14.9			
sc	6	16.2	13.9	15.7	16.5	17.8
β -tin	6	15.5	13.4		15.5	17.2
bcc	8	14.7	15.4	17.1	14.7	17.1
Simple hexagonal	8	15.0	13.4		16.5	18.1
fcc	12	14.7	16.1	17.0	14.8	17.8
hcp	12	14.5	15.4	15.5	14.8	18.6

^a [8, 12].

^b [8, 23, 45].

Table 6. Prediction of c/a ratios for fully relaxed crystal phases. For each crystal phase comparison is made for LDA, our model, and the SW, Tersoff and EDIP models.

Structure	LDA	Our model	SW ^a	Tersoff ^a	EDIP ^b
Hexagonal diamond	1.633 ^c	1.633	1.633	1.633	1.633
bct5	1.800 ^d	2.335			
β -tin	0.55 ^c	0.555	0.561	0.524	
Simple hexagonal	0.94 ^c	0.925	0.918	0.967	
hcp	1.633 ^c	2.043	0.884	1.633	2.130

^a [8].

^b [12].

^c [45].

^d [23].

with the possible exception of the bct5 phase, which is described in [23, 24]. This agreement is especially notable given that none of these structures (except cubic diamond) were included in the fitting database. Under pressure, our model converts from diamond to simple hexagonal. The correct phase transformation, seen in experiments and predicted by *ab initio* calculations, is from diamond to β -tin, and then to simple hexagonal at a higher pressure. The tight-binding model [13] actually predicts these transitions in the correct order. The Tersoff model also predicts the transition to β -tin as pressure is applied; it was fit in part to crystal phase energetics. The experimentally observed R8 phase [25, 26] is not stable in our model, but gives the closely related BC8 geometry when relaxed.

Tables 5 and 6 give additional information about the equilibrium volume of each phase, and the c/a ratios for the relaxed unit cells of applicable phases (hexagonal diamond, bct5, β -tin, simple hexagonal, and hcp). Our model gives too low volumes for simple hexagonal and β -tin, but it does quite well in predicting the c/a ratios for these two phases. The Tersoff model does especially well in predicting the equilibrium volumes of the various phases, but is less accurate in predicting the c/a ratios of the simple hexagonal and β -tin phases.

One important detail we want to address here is the energetics of the hexagonal diamond structure. It is intimately related to the stacking fault energy, which is generally zero for short-

Table 7. Generalized stacking fault energies (in J m^{-2}) for the unrelaxed glide and shuffle $\{111\}$ planes, computed using LDA, EDIP, SW and our model.

		LDA ^a	EDIP ^b	SW ^b	Our model
Glide	(112)	2.51	3.24	4.78	3.47
	(110)	24.71	13.45	26.17	26.45
Shuffle	(110)	1.84	2.16	1.38	1.22

^a [27].^b [12].

ranged potentials, e.g. EDIP, SW, and Tersoff, which do not extend beyond the second nearest neighbour. However, in our model the pair potential $\phi(r)$ extends up to 4.5 \AA and is negative at the third-neighbour distance across a stacking fault, while it is zero at the third-neighbour distance in unfaulted silicon. This leads to a slightly negative stacking fault energy which renders the hexagonal diamond structure more stable than the ordinary diamond structure by less than 0.01 eV per atom. In reality the latter is more stable than the former by 0.016 eV per atom. We feel that the error of 0.025 eV per atom is small, in the light of the simplicity of this model. Larger errors than this are observed for relative energies of other phases (cf table 4). In situations where a stacking fault is present—such as separating two partial dislocations—the previous models which give zero stacking fault energy will behave qualitatively the same as our model, in that the partial dislocations will separate to infinity in order to minimize elastic energy.

It is commonly perceived that the energetics of dislocations are intimately related to that of stacking fault energies. Hence it would be expected that errors in the latter would affect the quality of the model in describing the former. In fact, EDIP was fitted in part to generalized stacking-fault (GSF) energies, the energies for displacements along the glide and shuffle set of the $\{111\}$ glide plane [27]. However, despite the fact that these were not included in our fitting database, and given the aforementioned negative stacking fault energy problem, our model seems to provide a better overall description of both GSF and dislocation energies, in comparison with EDIP and SW models (cf table 7).

We computed reconstruction energies for 30° and 90° partial dislocations. For these dislocations, we constructed unit cells containing two partials with opposite Burger's vectors, connected across the cell by a stacking fault. The cells were chosen with nonorthogonal lattice vectors so that the dislocations would not align to form a low-angle grain boundary. Dangling bonds along the dislocation lines were allowed to dimerize. We considered symmetric configurations (where the dimer tilt directions were the same on each of the dislocations in the cell) as well as asymmetric configurations. Our results are summarized in table 8. Notably, our model correctly predicts that 'asymmetric' bonding is more stable for the 90° reconstruction, which EDIP does not. Also, it predicts the energetics of the 90° partial much more accurately in the smaller, 48-atom, cell. In this cell the interaction between the dislocation lines is greater, because their separation is reduced. The 90° partial dislocation also has a double-period reconstruction, which was proposed by Benetto *et al* [28]. We find this reconstruction to be favoured over the single-period reconstruction by 18 MeV \AA^{-1} , using a 192-atom unit cell; we computed a value of 73 MeV \AA^{-1} using LDA with the same geometries, while EDIP gives 165 MeV \AA^{-1} . The details of our dislocation calculations will be published in an forthcoming work [29].

Neither the SW model [4] nor the Tersoff models [9] describe partial dislocation reconstructions well [12]; the SW model gives reconstruction only for the 30° partial

Table 8. Energies of dislocation reconstructions (in eV per reconstruction bond) for the 30° and 90° partial dislocations, computed using LDA, our model and the EDIP potential. These are computed using a cell containing two dislocation lines, separated by a stacking fault. The symmetric case means that the tilt of dimers is in the same direction on both lines, while the asymmetric case refers to tilt on opposite directions; 90° partial calculations are for the single period reconstruction.

Configuration	LDA ^a (eV)	Our model (eV)	EDIP ^b (eV)
30° partial 96-atom cell	1.02	1.21	0.67
90° partial 48-atom cell symmetric case	0.27	0.20	0.05
90° partial 48-atom cell asymmetric case	0.41	0.23	0.02
90° partial 192-atom cell symmetric case	0.37	0.22	0.26
90° partial 192-atom cell asymmetric case	0.39	0.23	0.25

^a LDA values we computed using VASP.

^b [12].

Table 9. Formation energies for the lattice vacancy and interstitial silicon in different configurations. All defect energies are computed for fully relaxed configurations. We have chosen to compare them with the energy of the T⁺⁺ interstitial, which is the most stable charge state of the T interstitial when the Fermi level is at midgap.

Configuration	LDA ^a (eV)	Our model (eV)	EDIP ^b (eV)	Tersoff ^b (eV)
Vacancy	3.73	3.30	3.22	3.70
H interstitial	3.33	3.21	4.16	4.61
X interstitial	3.24	3.13	3.35	
T ⁺⁺ interstitial	3.23	3.11	4.05	3.45
T ⁺ interstitial	3.24			
T interstitial	3.52			
T* configuration ^c		3.00		

^a LDA values we computed using VASP.

^b [12].

^c Relaxed configuration with interstitial atom displaced from T by 0.40 Å in the direction of H.

dislocation, while Tersoff gives reconstruction only for the 90° partial dislocation. EDIP was the first interatomic silicon potential to describe both reconstructions.

For point defects the predictions of our model are summarized in table 9. In this fit, we have chosen to fit to the formation energy of the doubly-charged T⁺⁺ LDA interstitial rather than the neutral charge state of the tetrahedral interstitial, because T⁺⁺ is the most stable charge state when the Fermi level is at midgap. The lowest-energy interstitial for our potential is displaced by 0.40 Å from T in the direction of H. We have denoted it as T* in table 10; it is a spurious minimum which we find is not present in LDA. We generated these values using the VASP plane-wave pseudopotential code, which was developed at the Technical University of Vienna [30]. This code implements the Vanderbilt ultrasoft pseudopotential scheme [31],

Table 10. Relaxation energies for the lattice vacancy, and interstitial silicon in the H and T interstitial sites. We have chosen to compare them with the energy of the T^{++} interstitial, which is the most stable charge state of the T interstitial when the Fermi level is at midgap.

Configuration	LDA ^a (eV)	Our model (eV)	EDIP ^b (eV)	Tersoff ^b (eV)
Vacancy	0.39	0.55	0.25	0.4
H interstitial	0.80	0.41	2.70	3.61
T^{++} interstitial	0.44	1.20	6.52	3.47
T^+ interstitial	0.42			
T interstitial	0.39			

^a LDA values we computed using VASP.

^b [12].

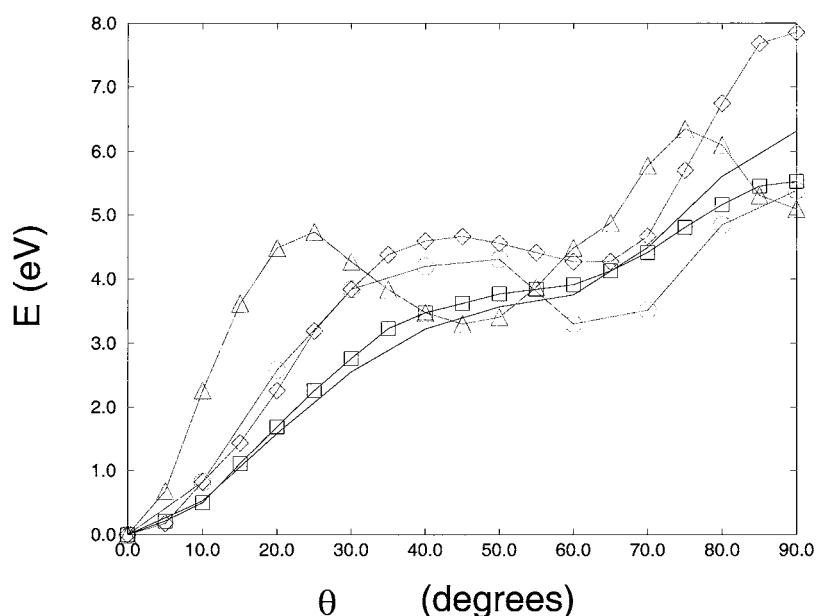


Figure 6. Energy of the unrelaxed concerted exchange path for our model (solid line), LDA (line with squares), EDIP (line with circles), Tersoff (line with triangles), and SW (line with diamonds). Data for LDA, EDIP, Tersoff and SW are from [8].

as supplied by Kresse and Hafner [32]. We computed these energies using large 128- and 256-atom unit cells. All the energies we quote are the true LDA values, with no corrections, meaning that they are computed with the Fermi level at the middle of the LDA gap. We also note that one model for corrections discussed in [33] still finds X and T^{++} nearly equal in energy to one another.

The point defect energies in table 9 are for relaxed defects; the relaxation energies of the vacancy, H interstitial, and the T interstitial are compared in table 10 for our model, EDIP, Tersoff and LDA. These energies are the energy difference between the ideal, unrelaxed, defect geometry, and the corresponding fully relaxed geometry, with zero forces and the same symmetry as the ideal geometry. Again the performance of our model is very good.

We also consider another point defect property: the concerted exchange process by which two silicon atoms exchange positions in the cubic diamond lattice. We have considered the unrelaxed concerted exchange, described in [34], in which a pair of atoms rotate about the

Table 11. Binding energy for global minimum-energy structures with two to five silicon atoms, as experimentally determined, and computed using an *ab initio* method, our model, Tersoff, and our previously published tight-binding model.

N	Experiment (eV)	<i>Ab Initio</i> ^a (eV)	Our model (eV)	Tight-binding ^b (eV)	Tersoff ^c (eV)
2	3.21 ^d	3.62	2.57	3.40	2.67
3	7.6 ± 0.2^e	7.82	6.11	7.21	5.33
4		12.36	9.69	12.03	8.64
5		16.50	13.37	16.09	12.44

^a [35].^b [13].^c [8].^d [47].^e [48].

midpoint of their bond while all other atoms in the lattice are fixed. The energy along this path is shown in figure 6, and compared to LDA, EDIP, Tersoff and SW values. While EDIP was fitted to LDA concerted exchange numbers, we included no such numbers in our fitting.

Clusters of between two and five atoms were included in the fitting database. Our potential finds global minima for these structures with the geometries of an equilateral triangle, a square, and a pyramid, while the corresponding *ab initio* result gives an equilateral triangle, a rhombus, and a trigonal bipyramid [35]. Our binding energies are compared to experimental values, *ab initio* results, Tersoff and tight-binding in table 11. It appears that our model has fairly good accuracy for even these low coordination structures (number of neighbours $Z = 1-4$). In fact, for the dimer our model predicts a bond length of 2.29 Å, while the corresponding *ab initio* result is 2.30 Å. While our geometries are not correct for four and five atoms, they are similar in shape and coordination to the correct global minima. In this case again, the tight-binding model [13] is somewhat more accurate in predicting cluster geometries and energies, predicting an isosceles triangle, a rhombus, and a trigonal bipyramid for the geometries.

The (100) silicon surface has a 2×1 reconstruction in which dangling bonds form dimers. In LDA the energy of this reconstruction is -1.9 ± 0.1 eV per dimer [36]. Our model shows very good agreement, giving an energy of -1.84 eV per dimer. Tersoff gives a value of -1.52 eV per dimer [8], while no value has been published for EDIP. In LDA the dimers prefer to tilt, however, with a tilt energy of 0.12 eV per dimer. This Jahn–Teller distortion is a subtle electronic effect which is not reproduced by our model. The tight-binding model [13] gives a reconstruction energy of only -1.3 eV per dimer, but correctly reproduces dimer tilt.

We also considered the case of a silicon adatom on the dimer-reconstructed (100) surface, which Smith *et al* [37] considered using density functional theory and the Tersoff and SW models. They reported LDA slab calculations with a binding energy of 4.71 eV at the global minimum ‘S’ site, and a binding energy of 3.85 eV at another ‘B’ site. Tersoff and SW both prefer the B site, with binding energies of 3.14 and 3.55 eV, respectively. In contrast, our model prefers the S site, with a binding energy of 3.19 eV. While our model does at least predict the correct binding site, its overall energy surface is only fair.

We have obtained the melting temperature for our model by performing molecular dynamics on a 4096-atom cubic diamond lattice with six free (100) surfaces for 50 ps at various temperatures. The free surfaces allow the liquid phase to have a different volume than the crystal. We used the Verlet algorithm and a 1 fs time step. The sample melted at $T_m = 1250 \pm 50$ K, 25% below the experimental melting point $T_m = 1683$ K.

We have also simulated the liquid phase at $T = 1800$ K using our model. Our model predicts the liquid to be 30% more dense than the solid phase, while in reality silicon becomes

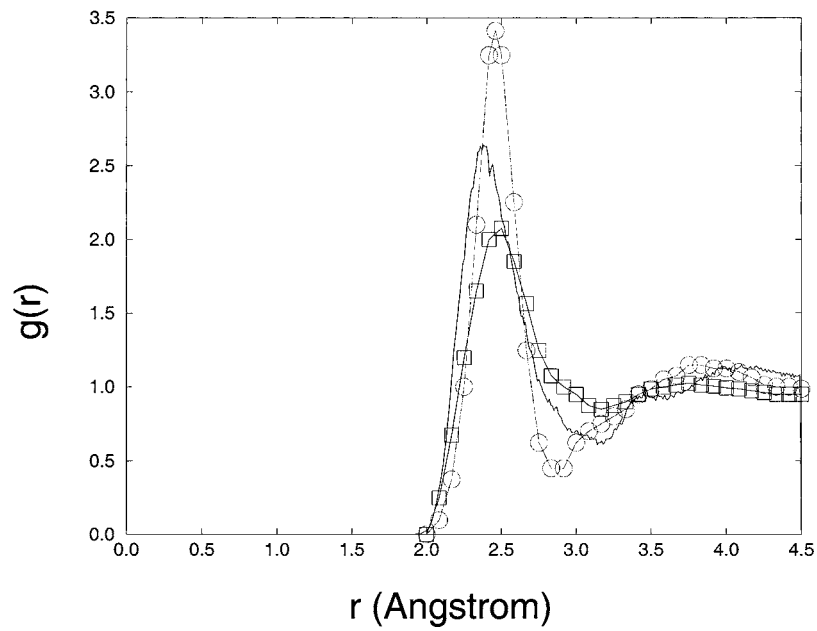


Figure 7. Pair-correlation function for the liquid at $T = 1800$ K for our model (solid line), compared with EDIP ([8], line with circles) and LDA ([32], line with squares).

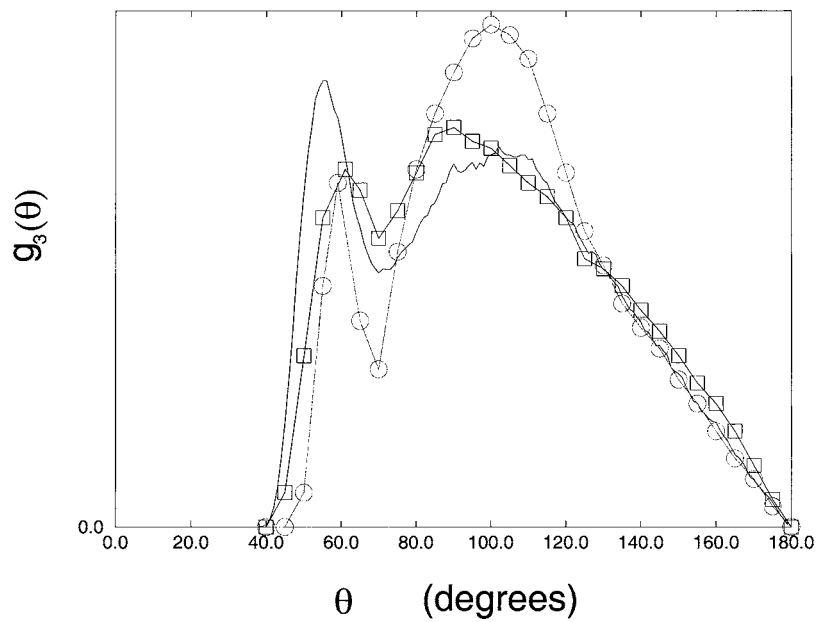


Figure 8. Bond-angle distribution for the liquid at $T = 1800$ K for our model (solid line), compared with EDIP ([8], line with circles) and LDA ([32], line with squares).

only 10% more dense upon melting [38]. The pair-correlation function $g(r)$ for the simulation is shown in figure 7. The coordination of the liquid (the average coordination, for neighbours

Table 12. Formation energies per interstitial in eV of small interstitial clusters, interstitial chains, and planar {311} defects. Two distinct configurations—compact and elongated—are considered for three-interstitial I_3 and four-interstitial I_4 clusters. The interstitial chain is composed of a row of X interstitials in the [110] direction. The periodicity of the planar {311} defects in the $[2\bar{3}\bar{3}]$ direction is denoted by $/\dots/$ according to the conventions in [40].

	LDA ^a	Our model	Tight-binding ^b	EDIP
Compact I_3	1.90	2.01	2.61	2.95
Elongated I_3	2.26	2.11	2.70	2.65
Compact I_4	1.60	1.43	2.08	2.33
Elongated I_4	1.99	1.86	2.47	2.53
I -chain	1.02	1.07	1.95	1.96
$/11/$	0.71	0.75	1.22	1.40
$/10/$	0.76	1.14	1.40	1.72

^a [40].

^b Values are computed by using tight-binding parameters from [13].

closer than the first minimum r_m in $g(r)$), is 7.0, compared with an experimental value of 6.4. EDIP gives a coordination of 4.5 under similar conditions [12], and gives a liquid which is less dense than the solid. The normalized distribution of angles between pairs of bonds shorter than r_m , $g_3(\theta, r_m)$, is shown in figure 8. It is bimodal with maxima at 56° and 102° ; the corresponding *ab initio* distribution is bimodal with peaks near 60° and 90° [39]. EDIP first captured the bimodal shape of g_3 under realistic simulation conditions [12]. Except for the fact that our model overestimates the density of liquid silicon, our model predicts $g(r)$ and $g_3(\theta)$ equally as well as EDIP in comparison to *ab initio* results [12]. Perhaps because of the low coordination of the EDIP liquid, it is easy to quench it into a nearly fourfold coordinated amorphous state [12].

Table 12 presents formation energies of interstitial complexes—small clusters, interstitial-chain and planar {311} defects. The formation energies are normalized by the number of interstitials contained in a defect. A stability hierarchy from small to extended interstitial defects established by LDA calculations [40] is reproduced by our model, tight-binding [13] and EDIP. The relative stability between compact and elongated configurations for small clusters I_3 and I_4 is correctly described by our model and tight-binding, while EDIP finds elongated configurations as the ground structure for such small clusters as I_3 . The formation energies predicted by our model are in excellent agreement with those determined by LDA of any size and shape. The typical errors of our model are less than 1% for the bond lengths of the defect cores and 5% for the bond angles.

4. Conclusions

We have fitted a new interatomic potential for silicon which generalizes the EAM and SW functional forms. Our model contains many degrees of freedom which are fitted to a large database of first principles and experimental data. We have extensively compared our model to the EDIP potential [12], a recent state-of-the-art interatomic silicon potential. In almost all cases, the performance of our model was equal or better than EDIP.

Our model provides a reasonable description of energetics for all atomic coordinations from the dimer ($Z = 1$) to fcc ($Z = 12$). It is fitted to accurately reproduce phonons and elastic constants, as well as point defect energetics. It provides a good description of dislocation reconstruction energetics for both the 30° and 90° partial dislocations, and accurately predicts the reconstruction energy for the 2×1 reconstruction of the (100) surface. So far, for the

properties we have tested our model produced encouraging results, although further testing is warranted.

At this point it is useful to summarize the situations where it is known that the model does not work well. These problems should not preclude use of the model, as previous models (SW, Tersoff and EDIP) also fail in a variety of cases. Some of the problems with the MEAM model have already been described in the text, i.e. the liquid is too dense, and there are some problems with the description of various crystal phases. Most notably, the hexagonal diamond structure is too stable, the R8 structure is not stable, and some of the structures such as β -tin tend to be too dense. Two of the most serious problems with the model, however, are shared by the SW, Tersoff, and EDIP models. The first major problem is that there is no charge transfer and no Coulombic interaction in the model; in a real silicon crystal there is a Fermi level and defects can have different charge states. The second major problem is that the model does not describe brittle fracture very well.

In conclusion, we have succeeded in fitting a potential form (MEAM) that accurately describes the bonding in silicon, which with different parameters is known to describe late transition metals well. We are thus hopeful to be able to extend our methodology to fitting more complicated elemental systems, such as early transition metals as well as multicomponent systems.

Acknowledgments

We thank Professor J W Wilkins for helpful suggestions on the manuscript. The work was performed under the auspices of the Department of Energy (DOE) at Lawrence Livermore National Laboratory (contract W-7405-ENG-48) and at Los Alamos National Laboratory (contract W-7405-ENG-36) with support from the DOE Office of Basic Energy Sciences, Division of Materials Science (OBES-DMS). The work at Ohio State University was supported by the National Science Foundation and by the DOE OBES-DMS (grant F602-99-ER45795).

References

- [1] Pettifor D G and Oleinik I I 2000 *Phys. Rev. Lett.* **84** 4124
- [2] Norskov J K and Lang N 1980 *Phys. Rev. B* **21** 2131
Stott M J and Zaremba E 1980 *Phys. Rev. B* **22** 1564
- [3] Daw M S and Baskes I 1984 *Phys. Rev. B* **29** 6443
Daw M S and Baskes I 1983 *Phys. Rev. Lett.* **50** 1285
- [4] Stillinger F and Weber T 1985 *Phys. Rev. B* **31** 5262
- [5] Baskes M I and Johnson R A 1994 *Modelling Simul. Mater. Sci. Eng.* **2** 147
Baskes M I 1997 *Mater. Chem. Phys.* **50** 152
Baskes M I 1999 *Mater. Sci. Eng. A* **261** 165
- [6] Baskes M I 1992 *Phys. Rev. B* **46** 2727
- [7] Pasianot R, Farkas D and Savino E J 1991 *Phys. Rev. B* **43** 6952
- [8] Balamane H, Halicioglu T and Tiller W A 1993 *Phys. Rev. B* **46** 2250
- [9] Tersoff J 1986 *Phys. Rev. Lett.* **56** 632
Tersoff J 1988 *Phys. Rev. B* **37** 6991
Tersoff J 1988 *Phys. Rev. B* **38** 9902
- [10] Biswas R and Hamann D R 1987 *Phys. Rev. B* **36** 6434
Biswas R and Hamann D R 1985 *Phys. Rev. Lett.* **55** 2001
- [11] Justo J F, Bazant M Z, Kaxiras E, Bulatov V V and Yip S 1997 *Materials Research Society Proc.* vol 469, ed T Diaz de la Rubia et al (Pittsburgh, PA: Materials Research Society)
- [12] Bazant M Z, Kaxiras E and Justo J F 1997 *Phys. Rev. B* **56** 8542
Justo J F, Bazant M Z, Kaxiras E, Bulatov V V and Yip S 1998 *Phys. Rev. B* **58** 2539

- [13] Lenosky T J, Kress J D, Kwon I, Voter A F, Edwards B, Richards D F, Yang S and Adams J B 1997 *Phys. Rev. B* **55** 1528
- [14] Ercolessi F and Adams J B 1994 *Europhys. Lett.* **26** 583
- [15] Liu X-Y, Adams J B, Ercolessi F and Moriarty J A 1994 *Modelling Simul. Mater. Sci. Eng.* **4** 293
- [16] Liu X-Y, Ohotnicky P P, Adams J B, Rohrer C L and Hyland R W 1997 *Surf. Sci.* **373** 357
Liu X-Y and Adams J B 1998 *Acta Mater.* **46** 3467
- [17] Liu X-Y, Xu W, Foiles S M and Adams J B 1998 *Appl. Phys. Lett.* **72** 1578
- [18] Landa A, Wynblatt P, Siegel D J, Adams J B, Mryasov O N and Liu X-Y 2000 *Acta Mater.* **48** 1753
Landa A, Wynblatt P, Siegel D J, Adams J B, Mryasov O N and Liu X-Y 2000 *Acta Mater.* **48** 3621 (corrigendum)
- [19] Press W H, Teukolsky S A, Vetterling W T and Flannery B P 1992 *Numerical Recipes in C: The Art of Scientific Computing* 2nd edn (Cambridge: Cambridge University Press)
- [20] Powell M J D 1965 *Comput. J.* **7** 303
- [21] Porter L J, Justo J F and Yip S 1997 *J. Appl. Phys.* **83** 5378
- [22] Richards D F and Adams J B 1995 *Proc. 1995 High Performance Computing Multiconference* (Phoenix, AZ: Society for Computer Simulation)
- [23] Kaxiras E and Boyer L L 1994 *Phys. Rev. B* **50** 1535
- [24] Boyer L L, Kaxiras E, Feldman J L, Broughton J Q and Mehl M J 1991 *Phys. Rev. Lett.* **67** 715
- [25] Pfrommer B G, Côté M, Louie S G and Cohen M L 1997 *Phys. Rev. B* **56** 6662
- [26] Piltz R O, Maclean J R, Clark S J, Ackland G J, Hatton P D and Crain J 1995 *Phys. Rev. B* **52** 4072
- [27] Kaxiras E and Duesbery M S 1993 *Phys. Rev. Lett.* **70** 3752
- [28] Bennetto J, Nunes R W and Vanderbilt D 1997 *Phys. Rev. Lett.* **79** 245
- [29] Bulatov V V, Lenosky T J and Diaz de la Rubia T at press
- [30] Kresse G and Hafner J 1993 *Phys. Rev. B* **47** RC558
Kresse G and Furthmüller J 1996 *Comput. Mater. Sci.* **6** 15–50
Kresse G and Furthmüller J 1996 *Phys. Rev. B* **54** 11 169
- [31] Vanderbilt D 1990 *Phys. Rev. B* **41** 7892
- [32] Kresse G and Hafner J 1994 *J. Phys.: Condens. Matter* **6** 8245
- [33] Harrison W A 1998 *Phys. Rev. B* **57** 9727
- [34] Pandey K C 1986 *Phys. Rev. Lett.* **57** 2287
- [35] Fournier R, Sinnott S B and DePristo A D 1992 *J. Chem. Phys.* **97** 4149
- [36] Ramstad A, Brocks G and Kelly P J 1995 *Phys. Rev. B* **51** 14 504
- [37] Smith A P, Wiggs J K, Jónsson H, Yan H, Corrales L R, Nachtigall P and Jordan K D 1995 *J. Chem. Phys.* **102** 1044
- [38] Glazov V M, Chizhevskaya S N and Glagoleva N N 1969 *Liquid Semiconductors* (New York: Plenum)
- [39] Štich I, Car R and Parrinello M 1991 *Phys. Rev. B* **44** 11 092
Car R and Parrinello M 1988 *Phys. Rev. Lett.* **60** 204
- [40] Kim J, Kirchhoff F, Wilkins J W and Khan F S 2000 *Phys. Rev. Lett.* **84** 503
- [41] Donohue J 1974 *The Structure of the Elements* (New York: Wiley)
- [42] Brewer L *Lawrence Berkeley Laboratory Report LBL-3720* (unpublished) (for the cohesive energy at 0 K)
Moore C E 1949 *Atomic Energy Levels (NBS Circular No 467)* vol I (Washington, DC: US Government Printing Office)
- [43] Madelung O and Schulz M (eds) 1987 *Landolt–Börnstein: Numerical Data and Functional Relationships Science New Series III*, vol 22a (New York: Springer)
Madelung O, Schulz M and Weiss H (eds) 1982 *Landolt–Börnstein: Numerical Data and Functional Relationships Science New Series III*, vol 17a (New York: Springer)
- [44] Weinstein B A and Piermarini G J 1975 *Phys. Rev. B* **12** 1172
- [45] Needs R J and Mujica A 1995 *Phys. Rev. B* **51** 9652
- [46] Adams G B, O’Keeffe M, Demkov A A, Sankey O F and Huang Y 1994 *Phys. Rev. B* **49** 8048
- [47] Huber K P and Herzberg G 1979 *Molecular Spectra and Molecular Structure. Constants of Diatomic Molecules* vol 4 (New York: Van Nostrand–Reinhold)
- [48] Chatillon C, Allibert M and Pattoret A 1975 *C. R. Acad. Sci., Paris C* **280** 1505